J Appl Electrochem (2013) 43:637–644
DOI 10.1007/s10800-013-0553-2

ORIGINAL PAPER

Performance and cycling of the iron-ion/hydrogen redox flow cell with various catholyte salts

Michael C. Tucker · Venkat Srinivasan · Philip N. Ross · Adam Z. Weber

Received: 21 February 2013 / Accepted: 29 April 2013 / Published online: 11 May 2013

Abstract A redox flow cell utilizing the Fe^{2+}/Fe^{3+} and H_2/H^+ couples is investigated as an energy storage device. A conventional polymer electrolyte fuel cell anode and membrane design is employed, with a cathode chamber containing a carbon felt flooded with aqueous acidic solution of iron salt. The maximum power densities achieved for iron sulfate, iron chloride, and iron nitrate are 148, 207, and 234 mW cm^{-2}, respectively. It is found that the capacity of the iron nitrate solution decreases rapidly during cycling. Stable cycling is observed for more than 100 h with iron chloride and iron sulfate solutions. Both iron sulfate and iron chloride solutions display moderate discharge polarization and poor charge polarization; therefore, voltage efficiency decreases dramatically with increasing current density. A small self-discharge current occurs when catholyte is circulating through the cathode chamber. As a result, a current density above 100 mA cm^{-2} is required to achieve high Coulombic efficiency (>0.9).

Keywords Redox flow cell · Flow battery · Iron hydrogen cell

1 Introduction

There is currently a resurgence of interest in redox flow cells for energy storage [1–4]. They may be suitable for a wide variety of applications, including: transmission and distribution upgrade deferral; improving grid reliability by levelizing intermittent generation assets such as wind and solar; premium back-up power; and, time-shifting generation or end-use of electricity to produce positive energy-cost arbitrage. Redox flow cells use electrochemically-active anolyte and catholyte species to store energy. Typically, the active species are dissolved in liquids that are pumped from reservoirs through the cell, which contains electrodes and an ion exchange or microporous membrane. System power and energy are independent, and each can be optimized for a specific application or use scenario. The primary qualifications for adoption of redox flow cells into the mix of grid technologies are cost, reliability, and safety.

In this study, we report development of the iron-ion/hydrogen redox flow-cell system, depicted in Fig. 1. In this system, the anode active species is hydrogen gas and the cathode active species is the Fe^{2+}/Fe^{3+} couple, present as an aqueous salt in the catholyte. During discharge, the hydrogen is oxidized to protons and the iron is reduced:

$$\text{Cathode} \quad 2Fe^{3+}_{(aq)} + 2e^- \rightarrow 2Fe^{2+}_{(aq)} \quad E_o = 0.77 \text{ V versus SHE} \tag{1}$$

$$\text{Anode} \quad H_2 \rightarrow 2H^+ + 2e^- \quad E_o = 0.00 \text{ V versus SHE} \tag{2}$$

$$\text{Over all reaction} \quad 2Fe^{3+}_{(aq)} + H_2 \rightarrow 2Fe^{2+}_{(aq)} + 2H^+ \quad E_o = 0.77 \text{ V} \tag{3}$$

Much of the technology developed for hydrogen/oxygen fuel cells is transferrable to this system, and we have taken the approach of adopting standard fuel cell materials and test methods for initial studies of the iron-ion/hydrogen flow cell system. In particular, we use hydrogen electrodes, cation exchange membranes, gas diffusion layers (GDLs), and auxiliary cell housing and components developed for proton-exchange membrane (PEM) fuel cells. Superficially, the

M. C. Tucker (✉) · V. Srinivasan · P. N. Ross · A. Z. Weber
Environmental Energy Technologies Division, Lawrence Berkeley National Laboratory, 1 Cyclotron Road, Berkeley, CA 94720, USA
e-mail: mctucker@lbl.gov

iron-ion/hydrogen system we report here is a PEM fuel cell with the air replaced by an aqueous iron-salt solution. The solution is pumped through the cathode chamber, and wets the GDL.

The primary motivation for developing the iron-ion/hydrogen flow-cell system is that the active materials offer low toxicity and cost relative to common flow-battery materials such as chromium, vanadium, bromine, chlorine, and lead. For example, iron chloride is two orders of magnitude less expensive than vanadium pentoxide [5]. These considerations may outweigh the relatively low theoretical open circuit potential (0.77 V), a benefit of which is that the full capacity is available well within the stability window of water. A secondary motivation is to leverage the highly developed technology of PEM fuel cells to accelerate development of this similar system.

Discharge operation of the iron-ion/hydrogen redox flow-cell system has been demonstrated previously [6–8]. The best performance to date is reported by Fatih, et al. [6]. They used an iron-sulfate solution, Nafion membrane, Pt/C anode, and carbon-felt cathode, obtaining 70 mW cm^{-2} peak power at room temperature and 170 mW cm^{-2} at 70 °C. Various schemes for regenerating Fe^{3+} from Fe^{2+} after discharge have been proposed, including: radiochemical oxidation [7], chemical methods [9], and biochemical pathways [8]. In this study, the polarization data for in situ regeneration of Fe^{3+} via electrochemical charging is reported for the first time.

There are many iron salts that may be considered for use in the iron-ion/hydrogen flow cell. Several simple salts that occur in both Fe^{2+} and Fe^{3+} forms may be suitable in an aqueous flow-cell system. Iron citrate and iron phosphate were ruled out because they display very low solubility in water. Ferricyanide was ruled out because reacts with acid to form toxic hydrogen cyanide. The primary candidates were thus selected to be iron chloride, iron sulfate, and iron nitrate, on the basis of solubility, safety, and cost. Other flow-cell systems utilizing the $Fe^{2+/3+}$ couple include the Fe–Cr, Fe–Br, Fe–Ti, Fe–V, and all-Fe systems. The choice of iron salts in these systems is typically iron-chloride [1, 4, 10–13] or iron-sulfate [12, 14]. Supporting electrolytes, including hydrochloric [11, 12] or sulfuric acid [6] or ammonium chloride [10] are often used to increase solution conductivity.

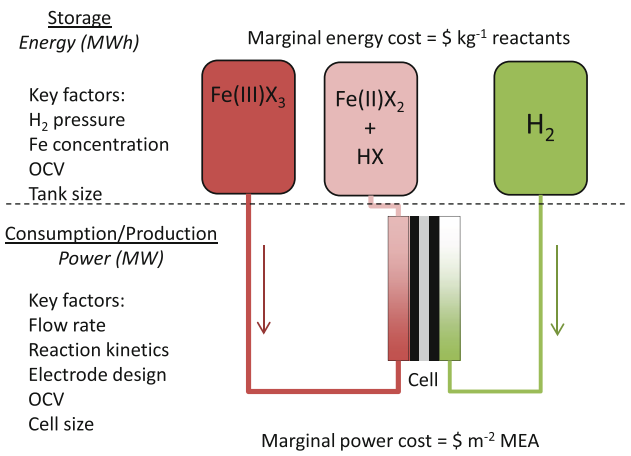

Fig. 1 Schematic representation of the iron-hydrogen flow cell system. *Arrows* indicate direction of flow during discharge

2 Experimental methods

A 10 cm^2 cell housing with graphite current collector blocks was used for all experiments (Fuel Cell Technologies 10SCH-PB). Moist hydrogen was supplied to the anode at 50 sccm through a water bubbler. Catholyte solutions were supplied to the cathode chamber at 40 mL min^{-1} by a peristaltic pump. The solution chamber was a glass jar, the solution was magnetically stirred and the headspace was flushed with nitrogen. The anode and cathode chambers were defined by PTFE gaskets, the thickness of which was selected to provide roughly 25 % compression of each GDL during cell assembly. All experiments were conducted at ambient temperature.

Aqueous catholyte solutions were prepared from high-purity iron nitrate (Alfa Aesar) and nitric acid (BDH); iron sulfate (Sigma-Aldrich) and sulfuric acid (BDH); and, iron chloride (BDH) and hydrochloric acid (BDH). Typical solutions were 0.7 M $Fe_2(SO_4)_3$/0.8 M H_2SO_4, 0.9 M $FeCl_3$/0.8 M HCl, 0.9 M $Fe(NO_3)_3$/0.8 M HNO_3. For self-discharge experiments, 2.7 M $FeCl_3$/0.8 M HCl was used.

Power density and polarization curves were obtained with a Fuel Cell Technologies test station. The MEA was a Nafion NR212 membrane with Pt/C (0.4 mg cm^{-2} Pt loading) printed on both sides (Ion Power). The anode GDL was a Sigracet 35BC and the cathode GDL was a Sigracet 35AA. Both anode and cathode flow fields were serpentine [15].

AC impedance, cycling, rate capability, efficiency, and self-discharge experiments were conducted with a Biologic VMP-3 potentiostat with 5 A booster. The cell consisted of Nafion NR212 membrane (DuPont) (pretreated by boiling 1 h each in hydrogen peroxide and then sulfuric acid), Sigracet GDE 10BC as the anode, and three layers of Sigracet GDL 10AA as the cathode (no Pt in the cathode chamber). The anode flow field was serpentine, and the cathode flow field contained only an inlet and outlet (catholyte flowed in one end of the chamber, through the GDLs, and out the other end), as described elsewhere [15].

Viscosity measurements were conducted on a Brookfield DVII+ Pro, with a CPE-52 cone and cup attachment.

3 Results and discussion

3.1 Cell performance

Solutions of the selected catholyte salts were prepared, each with the corresponding mineral acid as supporting electrolyte. The initial discharge performance for each catholyte solution is shown in Fig. 2. The OCVs observed for iron sulfate and iron chloride are consistent with, although slightly lower than the standard value of 0.77 V. The OCV observed for iron nitrate is considerably higher than expected. We suspect this is due to reduction of the nitrate ion to nitric oxide (standard potential 0.96 V vs. SHE). At OCV and during charging above 0.96 V (shown in this article) the solution did not change in appearance. During discharge of the iron nitrate solution in the region 0.75–0.95 V, however, the exit solution contained many bubbles of brown gas, presumed to be NO_2 (the oxidation product of nitric oxide and oxygen). As the potential continued dropping to ~0.5 V, the extent of bubble formation lessened. Below ~0.5 V, no bubbles were observed and the exit solution turned a dark green/black color (the solution was yellow/brown at all other potentials). We surmise that the high concentration of Fe^{2+} ion made available during deep discharge promoted a reaction that consumed the NO_2, thereby preventing formation of bubbles and producing a dark reaction product. The maximum power densities achieved for iron sulfate, iron chloride, and iron nitrate were 148, 207, and 234 mW cm^{-2}, respectively. The power density observed for iron sulfate at ambient temperature is considerably higher than that provided in previous reports [6].

Figure 3 shows AC impedance Nyquist plots for the various catholyte solutions at open circuit conditions. In each case, the total impedance can be attributed to roughly equal contributions from ohmic impedance, electrode polarization, and a low-frequency tail due to mass transport limitations. Note that the ohmic impedance of a Nafion membrane under 100 % relative humidity (RH) is roughly 0.15 Ω cm^2 [16]. The additional ohmic impedance observed in the present system may arise from contact resistance or uptake of catholyte species into the membrane [17, 18]; uptake of Fe^{3+} is known to reduce the conductivity of Nafion [19].

To assess the charging behavior, the catholyte solutions were galvanostatically discharged to 50 % state of charge (SOC) at 3 A so that there was sufficient Fe^{2+} species present to support charging. Figure 4 shows charge and discharge polarization for each catholyte. We believe this is the first report of charge polarization behavior for the iron-ion/hydrogen flow cell system. The OCVs are lower than shown in Fig. 2, consistent with the lower SOC. The discharge polarization is roughly linear, suggesting it is dominated by ohmic impedance, although in these systems mass-transfer limitations can appear ohmic as well if not

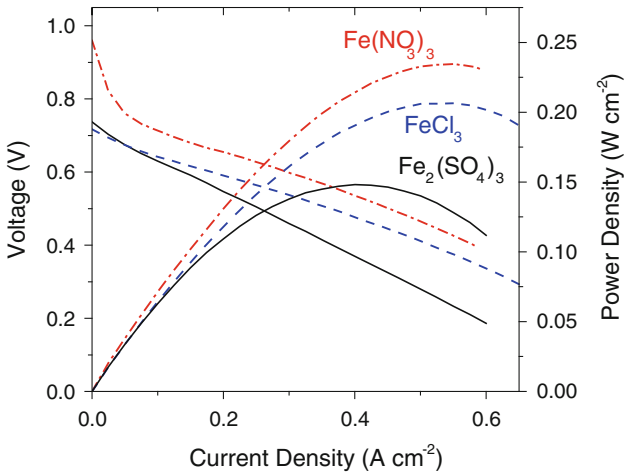

Fig. 2 Discharge polarization and power density for 0.7 M $Fe_2(SO_4)_3$/0.8 M H_2SO_4, 0.9 M $FeCl_3$/0.8 M HCl, and 0.9 M $Fe(NO_3)_3$/0.8 M HNO_3. Catholyte solutions were fully charged before starting the discharge (100 % state of charge)

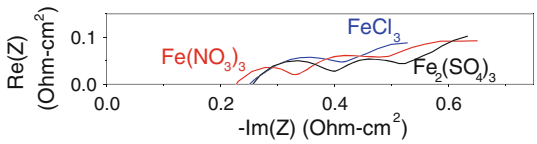

Fig. 3 AC impedance spectra for 0.7 M $Fe_2(SO_4)_3$/0.8 M H_2SO_4, 0.9 M $FeCl_3$/0.8 M HCl, and 0.9 M $Fe(NO_3)_3$/0.8 M HNO_3

near the limiting current [15]. In contrast, the charge polarization is concave, suggesting it is dominated by electrode activation or mass transport limitations. At the end of the charge polarization curve, the potential recovered to OCV very quickly (<0.50 ms), suggesting a mass-transport limitations are not significant factors. The steep charge polarization curve is a concern for applications of the flow cell in which energy must be captured quickly. Previous study shows good reversibility of the hydrogen electrode in the bromine/hydrogen flow cell [15] and PEM electrolyzer [20, 21], leading us to believe the hydrogen electrode is not responsible for the poor charge behavior observed in the present system. We cannot, however, rule out the possibility that the anode performance is degraded by the catholyte solution, e.g., via crossover of catholyte species. Previous study with the all-iron [10], and Fe/Cr [22] redox flow-cells do not report this asymmetry between charge and discharge behavior, however, the experimental conditions were limited to current densities below 150 mA cm^{-2}. An earlier study [23] of the redox behavior of the Fe^{2+}/Fe^{3+} couple in aqueous acidic media did show asymmetry between the anodic and cathodic polarizations, however, the data were collected near end-of-charge and end-of-discharge and concentration polarization likely overshadowed electrode kinetics. Future study will attempt to determine the cause of poor charge polarization. Note

also that the discharge performance in Fig. 4 is somewhat lower than shown in Fig. 2, suggesting that cell area specific resistance (ASR) is a function of SOC.

3.2 Cell cycling

Cells were assembled and cycled with each catholyte candidate. Cycling occurred galvanostatically, with voltage limits of 0.2–1.2 V. Because of the high overpotential upon charge discussed in Sect. 3.1, a low current density of 25 mA cm^{-2} was chosen. The first cycle for each catholyte is shown in Fig. 5 (discharge, followed by charge). In all cases, a single mildly sloping discharge plateau is observed, with relatively sharp transition to the terminal voltage at end of discharge. Discharge utilizations were 72, 82 and 90 % for iron nitrate, iron chloride, and iron sulfate, respectively. Utilization is discussed in more detail in Sects. 3.3 and 3.4. Upon charge, iron chloride and iron sulfate displayed moderately sloping charge plateaus with sharp transition to the terminal voltage at the end of charge. Both displayed significant Coulombic inefficiency, with more charge capacity required to recharge than was delivered during discharge. This is attributed to self-discharge as discussed in Sect. 3.4. In contrast, iron nitrate displayed a steeply sloping charge plateau and less charge capacity was required to recharge. This is attributed to depletion of the iron nitrate salt, as discussed in this article.

Cells with each catholyte were subjected to continuous galvanostatic cycling. The results are summarized in Fig. 6. Iron chloride was cycled approximately 50 times (more than 175 h total). There was a small loss of capacity during the first few cycles, after which the capacity was relatively stable. After cycling, the catholyte was replaced with fresh solution, and the capacity returned to a value similar to the

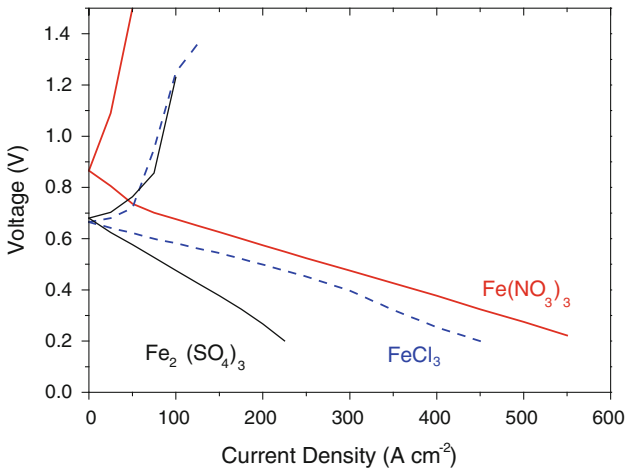

Fig. 4 Discharge and charge polarization for 0.7 M $Fe_2(SO_4)_3$/0.8 M H_2SO_4, 0.9 M $FeCl_3$/0.8 M HCl, and 0.9 M $Fe(NO_3)_3$/0.8 M HNO_3. Catholyte solutions were brought to 50 % state of charge before starting the discharge or charge data acquisition

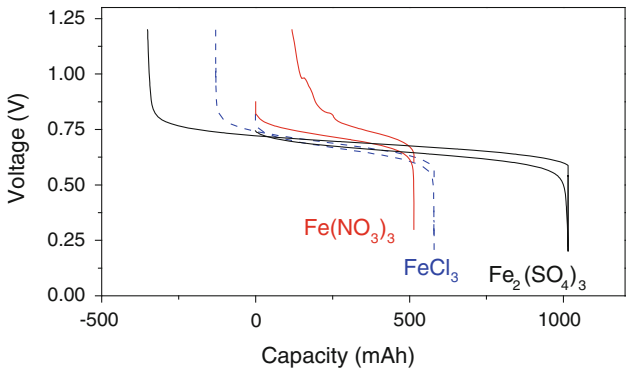

Fig. 5 Initial galvanostatic cycle (0.2–1.2 V, 25 mA cm^{-2}) for 0.7 M $Fe_2(SO_4)_3$/0.8 M H_2SO_4, 0.9 M $FeCl_3$/0.8 M HCl, and 0.9 M $Fe(NO_3)_3$/0.8 M HNO_3. Each solution was fully charged before starting the discharge/charge cycle shown

first cycle. This suggests the loss of capacity was due to depletion of the iron solution (a small amount of leakage was observed), and not due to irreversible degradation of the cell components (Nafion membrane, electrode materials, GDL, etc.). Iron sulfate was cycled 12 times. Note that the iron sulfate solution contains twice as much Fe^{3+} as the iron chloride solution, so each cycle was longer. After the first cycle, the discharge capacity was relatively stable for 100 h. In contrast, the capacity for iron nitrate rapidly decreased during the first few cycles. The catholyte solution was replaced, and the capacity recovered, again suggesting no catastrophic damage to the cell components. We surmise the iron was prevented from participating in the electrochemical reaction, perhaps via formation of inactive iron species in the catholyte or loss of nitrate via reduction to NO_2 as discussed above in Sect. 3.1. We did not undertake in-depth analysis of the failure mechanism, but rather chose to simply eliminate iron nitrate from further consideration.

3.3 Rate capability

In Sect. 3.1, it was observed that the overpotential during charging is quite high, and the discharge polarization behavior depends to some extent on SOC. Therefore, we undertook rate capability measurements in which the charge and discharge characteristics were observed during complete cycles at incremented current densities between 25 to 300 mA cm^{-2}. Several cycles were completed, starting at 25 mA cm^{-2} and with each cycle having higher current density than the previous one (see Fig. 7a). The final cycle again used 25 mA cm^{-2}, so that the first and last cycle could be directly compared. Thus, it could be confirmed that the cell had not suffered degradation or loss of capacity (via leakage, etc.) over the course of the whole cycling experiment. A typical cycle is shown in Fig. 7b. The cell was discharged and charged galvanostatically between 0.2 and 1.2 V. At the end of each galvanostatic

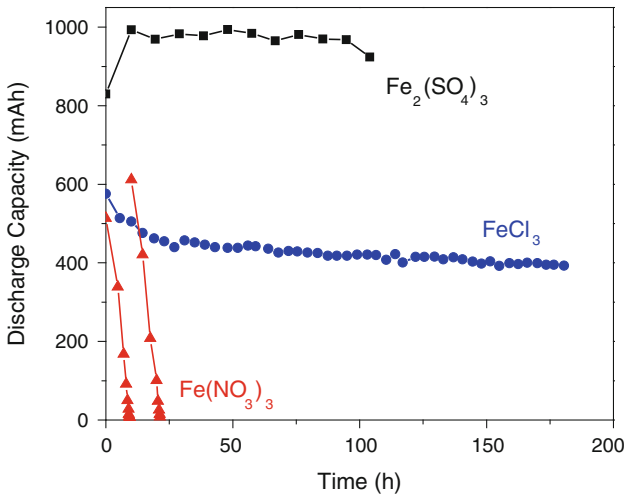

Fig. 6 Cycling stability during galvanostatic cycling (0.2–1.2 V, 25 mA cm^{-2}) for 0.7 M $Fe_2(SO_4)_3$/0.8 M H_2SO_4, 0.9 M $FeCl_3$/0.8 M HCl, and 0.9 M $Fe(NO_3)_3$/0.8 M HNO_3. After the first rapid depletion, the iron nitrate solution was replaced with fresh solution and cycled again

step, the cell was held at constant voltage until the current decayed to less than 15 mA cm^{-2} so as to utilize the full capacity. Rest periods of 2 min at open circuit occurred after each half-cycle.

The total capacity, Fig. 8a, was recorded as the sum of the capacities during the galvanostatic and potentiostatic portions. For both catholyte solutions, the charge capacity is higher than the discharge capacity, and the discrepancy is worse at low current density. This is attributed to self-discharge, as discussed in Sect. 3.4. For iron chloride, roughly 80 % of the theoretical capacity was achieved, and almost 100 % was achieved for iron sulfate. The average capacity was relatively independent of current density, suggesting the amount of active iron species was maintained over the course of the whole experiment.

Figure 8b shows the voltage efficiency, Coulombic efficiency, and energy efficiency for each complete cycle (including galvanostatic and voltage-hold portions). The Coulombic and energy efficiencies were taken as the full-cycle charge-to-discharge ratio of total mAh or mWh, respectively. The voltage efficiency is calculated as the energy efficiency divided by the Coulombic efficiency. For both catholyte solutions, the voltage efficiency decreases linearly and rapidly with increasing current density. Voltage efficiency above 90 % is achieved for the lowest current density. Coulombic efficiency was calculated as the ratio of the discharge and charge capacities over the entire cycle (sum of galvanostatic and potentiostatic portions). At low current density, the Coulombic efficiency is reduced due to self-discharge. At high current density, it is >95 %. Thus, there is a trade-off between Coulombic and voltage efficiency when selecting an operating current density.

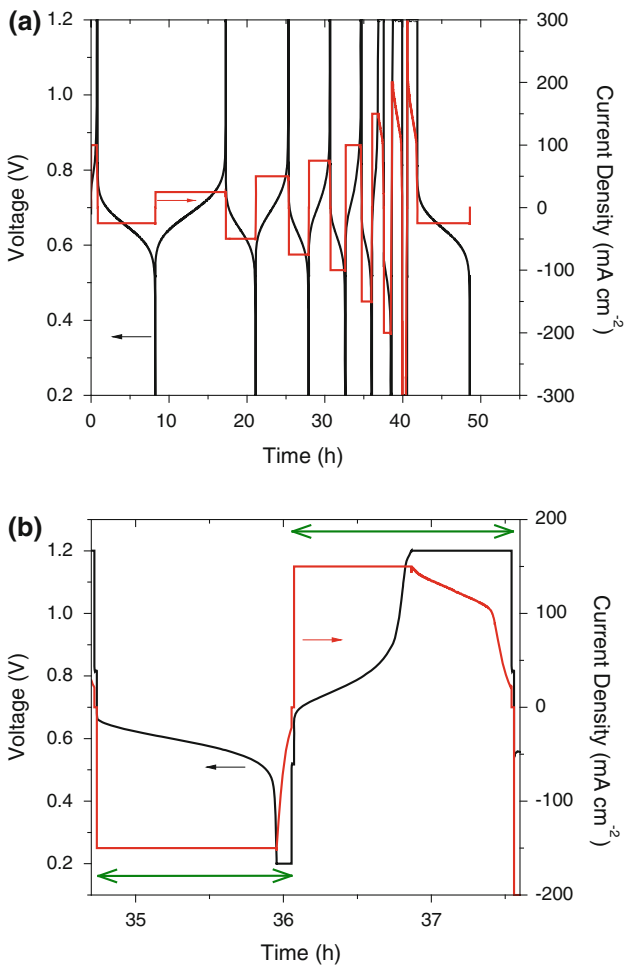

Fig. 7 **a** Incremented-current experiment for 0.9 M $FeCl_3$/0.8 M HCl. **b** A single cycle obtained with a galvanostatic current of 150 mA cm^{-2}. The half-cycles defined for calculating Coulombic efficiency are represented with *arrows*

Data from the galvanostatic portions were used to assess the rate capability of the cell. The galvanostatic utilization, Fig. 8c, was calculated as the ratio of galvanostatic capacity to total capacity (sum of galvanostatic and potentiostatic capacities) for each half-cycle. Thus, we can determine what portion of the capacity is available at a selected current density. For iron sulfate, the difference between charge and discharge rate capability is made very clear. Nearly all of the discharge capacity is available up to a current density as high as 200 mA cm^{-2}. The available charge capacity, however, drops precipitously above 75 mA cm^{-2}. The discrepancy is less for iron chloride, although the charge capacity is still compromised at lower current than the discharge capacity.

3.4 Self discharge

In Sects. 3.1 and 3.2, we reported a Coulombic inefficiency, with charge capacities generally being larger than

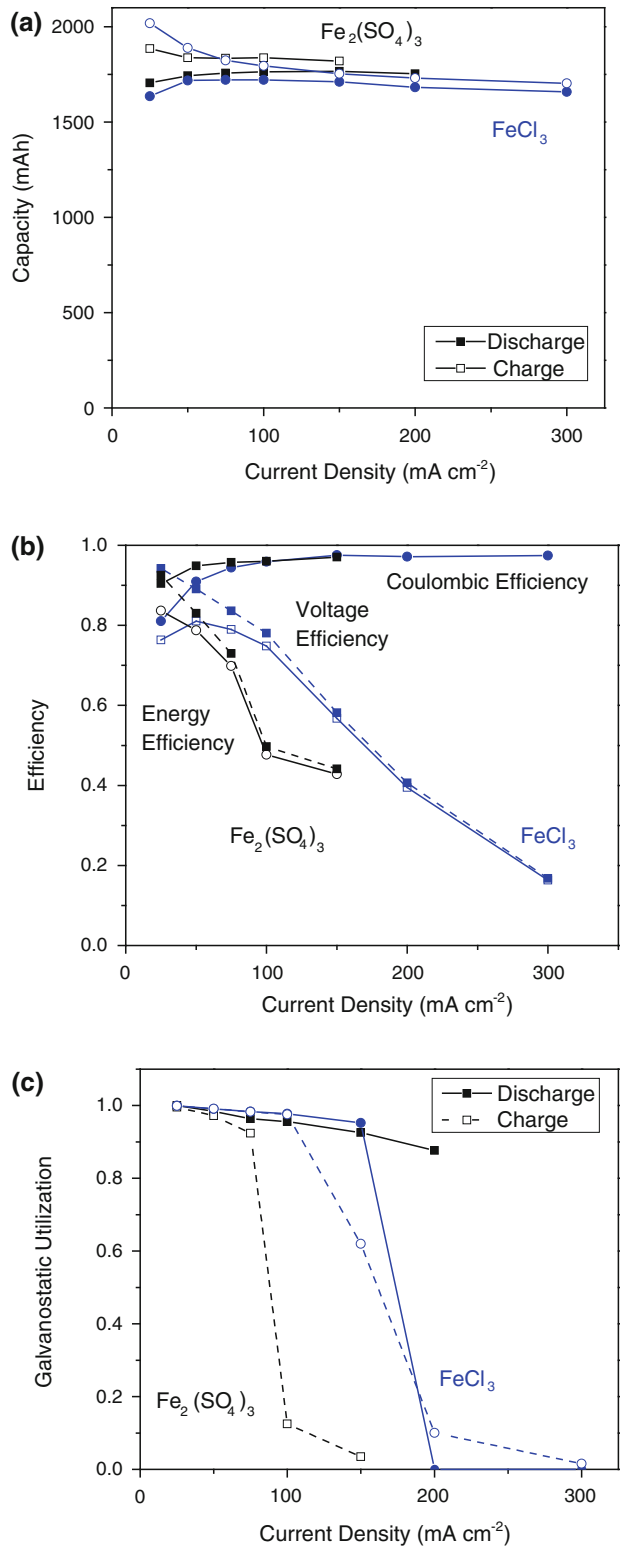

Fig. 8 Summary of results from incremented-current experiment for 45 mL 0.7 M $Fe_2(SO_4)_3$/0.8 M H_2SO_4 (*squares*), and 90 mL 0.9 M $FeCl_3$/0.8 M HCl (*circles*). **a** Discharge capacity (*solid symbols*) and charge capacity (*open symbols*). **b** Voltage efficiency (*closed symbols*, *dashed line*), Coulombic efficiency (*closed symbols*), and total energy efficiency (*open symbols*). **c** Galvanostatic utilization upon discharge (*solid symbols*) and charge (*open symbols*)

discharge capacities. The discrepancy is exacerbated at low current density. To elucidate the source of this "lost" charge, we proposed a wide variety of candidate mechanisms and conducted data analysis or simple experiments to support or refute each candidate.

The following list describes mechanisms that were ruled out, and the reason why:

(i) *Iron plating, uptake into Nafion, leakage of solution, or other iron sink;* solution volume was maintained over the course of all experiments, and the total capacity is stable during multiple cycles (see Fig. 8a)

(ii) *Spontaneous homogeneous chemical reduction of Fe^{3+} in catholyte solution;* long-term storage of catholyte on the shelf does not cause loss of discharge capacity

(iii) *Oxidation of GDL carbon in acidic media by Fe^{3+} as observed in* [24]; no weight loss of GDL observed after long-term cycling

(iv) *Side reactions not involving iron;* a cell was operated with aqueous acid catholyte (no iron), but no current could be sustained

(v) *Electrochemical side reactions driven by high current, or high (low) voltage at the end of charge (discharge);* cycles with higher current (and therefore more time at potentiostatic 0.2 or 1.2 V holds), are more efficient (Fig. 8b)

The candidate mechanism that best accounts for the observations is self-discharge reduction of Fe^{3+} when in the cell (inside the cathode chamber) via hydrogen permeation through the Nafion membrane. After charging fully, a cell with iron chloride catholyte was allowed to rest at open circuit, with catholyte circulating through the cathode chamber. Figure 9 shows that the cell potential decayed during the rest period of approximately 7 h. The cell was then fully re-charged, and the required charge corresponded to an average self-discharge current of 3.5 mA cm^{-2} during the rest period. This experiment was repeated with moist nitrogen flowing through the anode chamber, to eliminate the crossover flux of hydrogen through the membrane during the rest period. After 6 h, the nitrogen was replaced with hydrogen to determine OCV and self-discharge capacity. The required charge corresponded to an average self-discharge current of 0.6 mA cm^{-2} during the rest period; hydrogen permeation is so far the largest source of self-discharge.

The extent of self-discharge is linearly related to the time the catholyte spends in contact with the cell (in the cathode chamber) as shown in Fig. 10. This data was extracted from the same experiments shown in Fig. 8. The self-discharge capacity (difference between charge and discharge capacity) was determined for each cycle at various current densities, and is plotted as a function of total

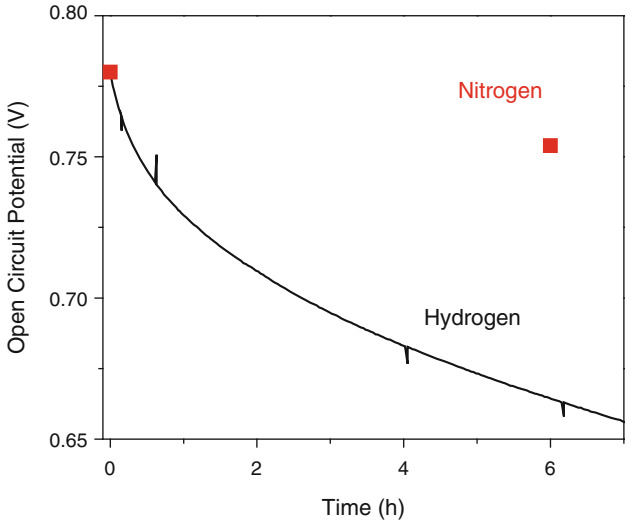

Fig. 9 Observation of self-discharge for 0.9 M $FeCl_3$/0.8 M HCl during rest at open circuit with catholyte continuously circulating through cathode chamber and moist hydrogen (*line*) or moist nitrogen (*symbols*) circulating through anode chamber. The anode gas was briefly switched from nitrogen to hydrogen to measure OCV at 6 h

cycle time (including both galvanostatic and potentiostatic steps). A linear relation is shown, with the slope corresponding to the average self-discharge current during the cycle. The slope is roughly 3 mA cm^{-2} for several iron-chloride catholyte solutions, consistent with the direct measurement of the self-discharge current above (see Fig. 9). Note that the slope is independent of iron-chloride concentration or solution volume (both of which are roughly linearly related to total cycle time), suggesting these variables do not impact the self-discharge rate.

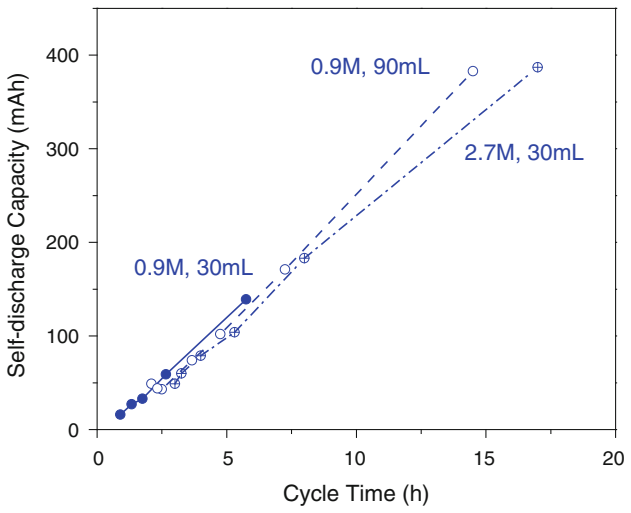

Fig. 10 Self-discharge capacity observed during various incremented-current cycles for 0.9 M $FeCl_3$/0.8 M HCl, and 2.7 M $FeCl_3$/0.8 M HCl

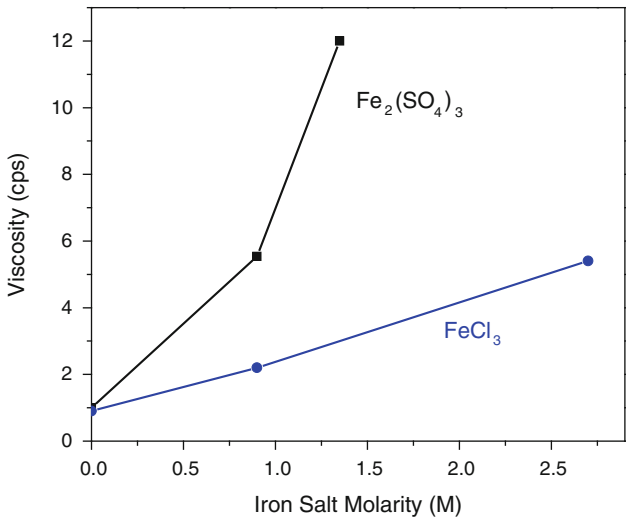

Fig. 11 Viscosity of various $Fe_2(SO_4)_3$/0.8 M H_2SO_4 and $FeCl_3$/0.8 M HCl solutions

Although self-discharge is not desirable, the fact that it only occurs when catholyte is flowing through the cell is encouraging. The self-discharge currents observed here are much lower than the charge and discharge currents expected for an optimized flow-cell system, so the impact on system efficiency should be minimal. The use of thicker or less permeable membranes would further reduce the impact of self-discharge.

3.5 Solution viscosity

During the course of experiments, it was noticed that the pressure drop through the cathode compartment varied significantly with the composition of the catholyte. Parasitic losses due to solution pumping can have an impact on any forced-flow system, and are of particular concern for designs having the catholyte flow forced through the GDL or other porous media (filters, etc.). A recent model of Vanadium-based redox flow batteries determined that pumping loss can be roughly 5–10 % of the total system losses [5]. Pumping losses are proportional to fluid viscosity; to ascertain the relative pumping losses for various catholyte compositions, the viscosity of iron-sulfate and iron-chloride solutions was measured. Figure 11 shows that the viscosity for iron-sulfate solutions increases much more rapidly with concentration than for iron-chloride solutions. This result should be considered in the selection of catholyte composition when designing a system.

4 Conclusions

The iron-ion/hydrogen redox flow cell has been tested with a variety of catholyte solution compositions. It was found

that iron-nitrate solutions rapidly lose capacity, possibly via reduction of the nitrate ion. Stable cycling was achieved with iron-chloride and iron-sulfate solutions. Although the cycling stability and utilization were marginally better for iron-sulfate solutions, the high viscosity and poor charge polarization lead us to conclude that iron chloride is the most promising salt of those studied herein.

All of the catholyte solutions tested here displayed moderate discharge rate capability, and poor charge rate capability. It is possible that this behavior is appropriate for certain charge-storage applications, but we anticipate significant improvement to the rate capability is required for commercialization of this system. Optimization of the cell and catholyte solution composition is a fruitful area for further study.

Acknowledgments Stanislaus Grosjean contributed to the design and fabrication of the experimental setup for this study. The authors thank Kyu Taek Cho for helpful discussion and guidance during the initiation of this study. We also thank John Kerr and Vincent S. Battaglia for fruitful discussion. This study was supported in part by the Assistant Secretary for Energy Efficiency and Renewable Energy, Fuel Cell Technologies Office, of the U.S. Department of Energy under contract number DE-AC02-05CH11231.

References

1. Ponce de Leon C, Frıas-Ferrer A, Gonzalez-Garcia J, Szanto DA, Walsh FC (2006) J Power Sources 160:716–732
2. Bartolozzi M (1989) J Power Sources 27:219–234
3. Weber AZ, Mench MM, Meyers JP, Ross PN, Gostick JT, Liu Q (2011) J Appl Electrochem 41:1137–1164
4. Skyllas-Kazacos M, Chakrabarti MH, Hajimolana SA, Mjalli FS, Saleem M (2011) J Electrohem Soc 158(8):R55–R79
5. Viswanathan V, Crawford A, Stephenson D, Kim S, Wang W, Coffey G, Thomsen E, Graff G, Balducci P, Kintner-Meyer M, Sprenkle V (2012) J Power Sources 10.1016/j.jpowsour.2012.12.023
6. Fatih K, Wilkinson DP, Moraw F, Ilicic A, Girard F (2008) Electrochem Solid State Lett 11(2):B11–B15
7. Yeager JF, Bennett RJ, Allenson DR (1962) Proceedings of the Annual Power Sources Conference, U.S. Army Signal Research and Development Laboratory, PSC Publications Committee 16:39
8. Karamanev D, (2009) US patent 7572546B2
9. Park KW, Han SB, Lee YW, Ko AR (2012) Korean patent application 10-1103847
10. Hruska LW, Savinell RF (1981) J Electrochem Soc 128:18–25
11. Wei X, Li L, Luo Q, Nie Z, Wang W, Li B, Xia GG, Miller E, Chambers J, Yang G (2012) J Power Sources 218:39–45
12. Li B, Li L, Wang W, Nie Z, Chen B, Wei X, Luo Q, Yang Z, Sprenkle S (2013) J Power Sources 229:1–5
13. Lopez-Atalaya M, Codina G, Perez JR, Vazquez JL, Aldaz A (1992) J Power Sources 39:147–154
14. Wen YH, Zhang HM, Qian P, Zhou HT, Zhao P, Yi BL, Yang YS (2006) J Electrohem Soc 153(5):A929–A934
15. Cho KT, Ridgway P, Weber AZ, Haussener S, Battaglia V, Srinivasan V (2012) J Electrochem Soc 159(11):A1806–A1815
16. Cooper KR (2010) J Electrochem Soc 157(11):B1731–B1739
17. Kusoglu A, Cho KT, Prato RA, Weber AZ (2013) Solid State Ionics, submitted
18. Weber AZ, Delacourt C (2008) Fuel Cells 8(6):459–465
19. Pupkevich V, Glibin V, Karamanev D (2007) J Solid State Electrochem 11:1429–1434
20. Altmann S, Kaz T, Friedrich KA (2011) Electrochim Acta 56:4287–4293
21. Hwang CM, Ishida M, Ito H, Maeda T, Nakano A, Hasegawa Y, Yokoi N, Kato A, Yoshida T (2011) Int J Hydrogen Energy 36:1740–1753
22. Codina G, Perez JR, Lopez-Atalaya M, Vazquez JL, Aldaz A (1994) J Power Sources 48:293–302
23. Giner J, Swette L, Cahill K (1976) NASA Contract NAS3-19760, NASA CR-134705
24. Dhooge PM, Stilwell DE, Park S-M (1982) J Electrohem Soc 129(8):1719–1724